Catalytic Desulfurization of Gasoline via Dehydrosulfidation

H. de Lasa,*,† R. Hernandez Enriquez,† and G. Tonetto‡

Faculty of Engineering Science, Chemical Reactor Engineering Centre, University of Western Ontario, London, Ontario, Canada N6A 5B9, and Chemical Engineering Department, PLAPIQUI (UNS−CONICET), Camino La Carrindanga Km 7, CC 717, (8000) Bahía Blanca, Argentina

This study presents a potentially attractive route for the desulfurization of gasoline via catalytic dehydrosulfidation, removal of hydrogen sulfide from sulfur-containing molecules. The proposed study involves thermodynamic calculations and experimentation in a fluidized riser simulator at the Chemical Reaction Engineering Centre (CREC) at the University of Western Ontario. A ZSM-5 catalyst was used because of its demonstrated performance for the dehydration of methanol, a parent reaction with an expected similar reaction network. The catalyst was characterized using several techniques, including (a) BET (surface area), (b) ammonia temperature-programmed desorption (concentration of acid sites), and (c) SEM-EDX (sodium content) at various stages of catalyst preparation. The catalytic dehydrodesulfidation reaction was studied using a model compound (ethyl mercaptan, EM) in *n*-octane (*n*-C_8) to represent sulfur-contaminated gasoline. The experimental data obtained were successfully fitted using a kinetic model representing the rate of disappearance of the sulfur-containing species.

1. Introduction

The refining industries are under constant pressure to achieve more rigorous standards with respect to product specification. These increased requirements are currently driven by environmental concerns.[1] Recent environmental regulations establish strict sulfur levels in transportation fuels.

Sulfur dioxide (SO_2) emissions can be traced to the combustion of sulfur species in transportation fuels. SO_2 emissions are of particular concern given that they are precursors of acid rain and sulfate aerosol formation, which contribute considerably to the total ambient fine particulate matter.

Sulfur in fuels also presents two problems for the auto industry: (a) loss of catalytic converter efficiency in car mufflers (i.e., catalyst poisoning), meaning that lower sulfur in fuels will result in an extended life for catalytic converters with reduced CO, NO_x, and hydrocarbon emissions, and (b) corrosion to parts of internal combustion engines caused by sulfur compounds.

Fluid catalytic cracking (FCC) gasoline contributes significantly to the total "gasoline pool" volume ranging from 25% to 40%. Gasoline coming from an FCC unit can have sulfur levels as high as 2000 ppm. Given that FCC gasoline accounts for more than 90% of the total sulfur in the gasoline pool, refineries must dramatically reduce sulfur in FCC gasoline to achieve the low sulfur levels required by the new legislation.

Several alternatives are currently being considered involving physical and/or chemical processes to address the issue of the sulfur content in gasoline,[2−4] and there is still a need for new technologies that can remove sulfur content, thereby reducing operating and capital costs.

The hydrotreating of FCC gasoline, or hydrodesulfurization (HDS), is a post-FCC treatment process performed to achieve low sulfur levels in gasoline. Catalysts typically used are CoMo/γAl_2O_3 and NiMo/γAl_2O_3.[5] Hydrodesulfurization reactions are exothermic and occur simultaneously with hydrogenation reactions. Hydrogenation reactions decrease the quality of gasoline because they convert olefins, which contribute to the gasoline octane number, into alkanes (paraffins). Desai[6] showed that there are no conditions in the HDS process under which hydrogenation can be completely eliminated. During HDS, sulfur is removed in the form of hydrogen sulfide (H_2S); however, H_2S can react with olefins, producing mercaptans.

Considering posttreatment desulfurization technologies that use chemical reaction techniques, it is apparent that the use of hydrogen adds significant costs. Thus, if one could envision a desulfurization process free of the hydrogen requirement, this process could offer major cost savings over HDS.

Chang and Silvestri[7] studied the conversion of methyl mercaptan (methane thiol) at 482 °C and 1 h^{-1} LHSV, obtaining conversions of 99%. The products obtained were hydrocarbons ranging from C_1 to C_{11} and H_2S. Unfortunately, about 27% of the carbon feed was converted to dimethyl sulfide. More detailed descriptions of the methanol-to-gasoline (MTG) process can be found elsewhere.[8−11] On this basis, one can expect that other mercaptans such as ethyl mercaptan can react over H−ZSM-5 catalyst to produce H_2S and hydrocarbon compounds within the gasoline range. This leads to the development of a novel process that can reduce sulfur content in the gasoline range without a reduction in the octane number index. In addition, all of these interesting prospects are achieved without having to use hydrogen as a co-reactant.

A few studies have already been published that support the use of H−ZSM-5 zeolite as a desulfurization catalyst. Collins et al.[12,13] used a fluidized-bed reactor with H−ZSM-5 catalyst to desulfurize hydrocarbons with no hydrogen addition. Organic sulfur compounds were converted to H_2S. The catalyst used contained 25% H−ZSM-5 zeolite, and the process could be used to desulfurize either light gases or gasoline streams, with light olefins being upgraded to more valuable gasoline-range materials. Up to 61% of the sulfur in the feed was converted to H_2S.

Desulfurization of thiophene on H−ZSM-5 was studied by Yu et al.[14] in a tubular reactor using alkanes (propane, *n*-hexane, and *n*-decane) as co-reactants. It was found that thiophene desulfurization increased with increasing alkane chain size. From this work and from previous studies by Biscardi and Iglesia,[15,16] it was found that thiophene does not alter the nature of alkane

* To whom correspondence should be addressed. E-mail: hdelasa@eng.uwo.ca.

† University of Western Ontario.

‡ PLAPIQUI (UNS−CONICET).

10.1021/ie0506825 CCC: $33.50
Published on Web 01/11/2006

reaction pathways on H−ZSM-5, but increases the selectivity to aromatics as a result of the selective reaction of alkane-derived species with unsaturated fragments formed during thiophene decomposition and thiophene desulfurization.

The present study considers the implementation of gasoline desulfurization via catalytic dehydrosulfidation. This innovative approach offers special advantages for the production of environmentally friendly gasoline and involves the utilization of ZSM-5 zeolite as the key catalyst. Potential benefits are (a) the elimination of hydrogen as a co-reactant, (b) a high degree of mercaptan dehydrosulfidation with no detectable levels of diethyl sulfide intermediate species, and (c) maintenance or even enhancement of the gasoline octane number index.

2. Experimental Section

2.1. Catalyst Preparation. The zeolites used in this research were synthesized in CREC laboratories, following the method originally proposed by Gabellica.[17] Then, the zeolites were pelletized into catalyst pellets in the 38−106-μm range, using the gel-and-grind technique. Pelletization was required to have a fluidizable catalyst. Pellets were prepared from a slurry containing three components: zeolite, filler, and binder.[18] Kaolin, $Al_2Si_2O_5(OH)_4$ (Aldrich), was used as the binder, and sodium silicate (LUDOX AS-40 colloidal silica, Aldrich, 40 wt % suspension in water) was employed as the filler. To avoid premature slurry gellification, sulfuric acid was used to keep the solution pH at 2. The three pellet components were supplied in amounts yielding pellets of 20 wt % zeolite, 40 wt % kaolin, and 40 wt % sodium silicate.

After the gel had formed, it was spread on a drying plate and calcined in an oven (4 h at 120 °C and 4 h at 560 °C). The calcination process collapses the kaolin crystalline phase, forming an amorphous phase. The solid mass was ground and sieved to obtain catalyst pellets in the appropriate size range.

The produced pellets were ion exchanged to obtain the protonic acid form of the ZSM-5 zeolite. Four ion exchanges were performed using 1 M NH_4NO_3 solution for 6 h at 80 °C. The catalyst pellets were washed and filtered three times between each ion exchange, and after that, a last wash was performed to ensure that all impurities had been removed completely. Finally, the catalyst pellets were calcined (4 h at 120 °C and 4 h at 560 °C) and sieved. Although this technique provides well-controlled zeolite loadings in catalyst pellets, it has the drawback of not yielding high-sphericity pellets.

2.2. Catalyst Characterization. 2.2.1. NH_3 Temperature-Programmed Desorption (TPD). The apparatus used for TPD tests was an AutoChem II analyzer from Micromeritics. The catalyst sample (ranging 0.1−0.3 g) set in a quartz container and degassed for 2 h at 500°C. The sample was brought to saturation level using an NH_3/He gas mixture (4.55% ammonia, 95.55% helium). The adsorption of ammonia was carried out for 1 h at 140 °C. The ammonia flow was then switched off and replaced by an inert purge gas (He) at a 50 mL/min rate for 1 h at the same temperature of ammonia adsorption. Then, the temperature was raised at a rate of 15 °C/min. As the temperature increased, the desorption process was followed with a thermal conductivity detector (TCD).

2.2.2. N_2 and Ar Isotherms. Nitrogen and argon adsorption measurements were carried out at 77 K on an ASAP 2010 automatic adsorption analyzer equipped with micropore options (from Micromeritics). Before the measurements, samples weighing from 0.1 to 0.3 g were degassed at 100 °C for 1 h and at 300 °C for 10 h. Adsorption isotherms were measured under relative pressures in the range from $\sim 10^{-6}$ to 1.

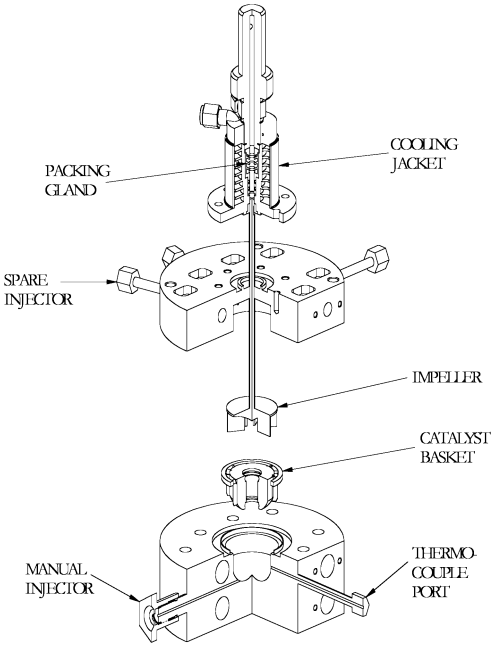

Figure 1. Schematic diagram of the CREC riser simulator: Quarter-section view, upper and lower shells exploded.

2.2.3. X-ray Diffraction (XRD). XRD analyses were performed using Co Kα radiation in a rotating-anode X-ray diffractometer over a 2θ range from 2° to 82°.

2.2.4. Scanning Electron Microscopy−Energy-Dispersive X-ray Spectroscopy (SEM-EDX). SEM-EDX analyses were carried out on a Hitachi S-4500 field-emission SEM equipped with an EDAX EDX system.

2.3. Catalytic Experiments. Experiments were performed using a CREC riser simulator.[19] A schematic diagram of a 52-cm^3 riser simulator is presented in Figure 1. The riser simulator consists of two outer shells, a lower section, and an upper section that permits the easy loading and unloading of the catalyst. This reactor was designed in such a way that an annular space is created between the outer portion of the basket and the inner part of the reactor shell. A metallic gasket seals the two chambers, and an impeller is located in the upper section. A packing gland assembly and a cooling jacket surround the shaft that supports the impeller. Upon rotation of the shaft, gas is forced outward from the center of the impeller toward the walls. This creates a lower pressure in the center region of the impeller, thus inducing flow of gas upward through the catalyst chamber from the bottom of the reactor annular region where the pressure is slightly higher. The impeller provides a fluidized bed of catalyst particles as well as intense gas mixing inside the reactor.

The riser simulator operates in conjunction with a series of sampling valves that allow, following a predetermined sequence, the injection of hydrocarbons and the withdrawal of products in short periods of time (see Figure 2). An Agilent 6890N gas chromatograph (GC) with a flame ionization detector (FID) and a mass-selective detector (MSD, Agilent 5973N) allows the quantification of reaction products using an HP-5 phenyl methyl siloxane capillary column with a length of 30 m, a nominal diameter of 0.32 mm, and a nominal film thickness of 0.25 μm. More details of the mechanical design of the riser simulator are given by Kraemer[20] and Pruski.[21]

A model compound, ethyl mercaptan, C_2H_6S (Alfa Aesar, CAS number 75-08-1), was selected as a key chemical species to evaluate the mercaptan conversion and to assess the reaction network. The gasoline fraction was simulated with *n*-octane (EM

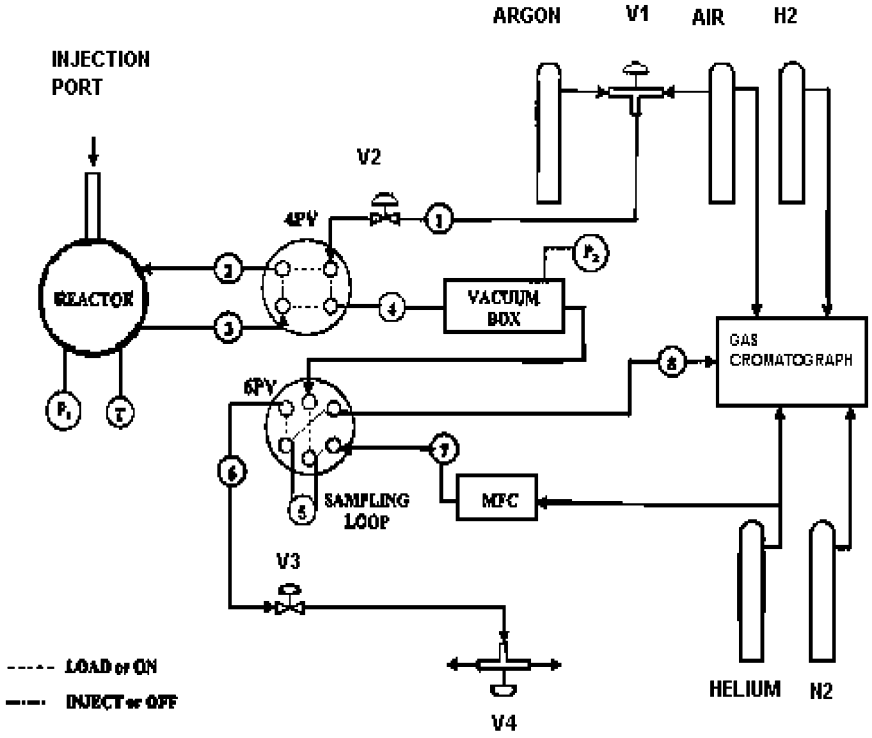

Figure 2. CREC riser simulator experimental setup.

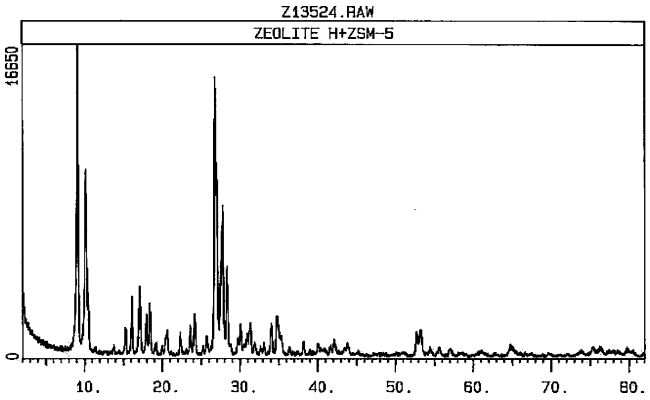

Figure 3. XRD pattern of H−ZSM-5 zeolite.

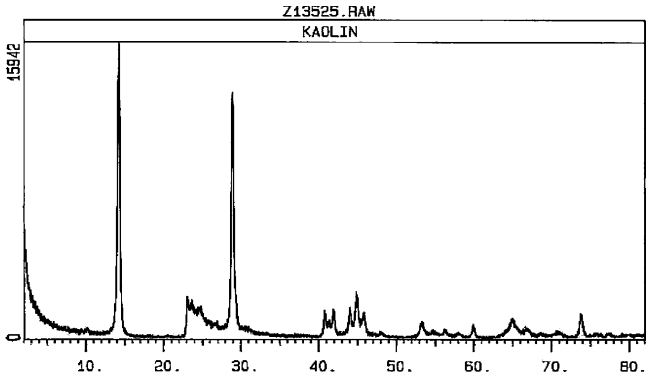

Figure 4. XRD pattern of kaolin.

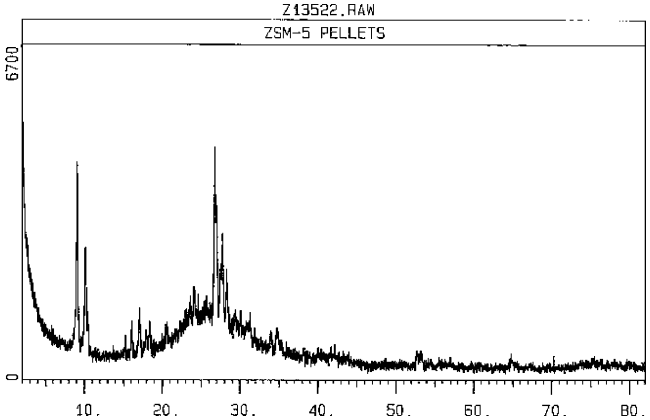

Figure 5. XRD pattern of H−ZSM-5 pellet.

Science, CAS number 111-65-9), a straight-chain hydrocarbon with a boiling point falling in the middle of the gasoline boiling range.

Mixtures of these compounds were reacted at different concentrations (5 and 10 wt %), three temperatures (350, 400, and 450 °C), and four contact times (10, 20, 40, and 60 s). The catalyst-to-oil ratio was set at C/O = 2.5. All experiments were repeated at least three times to ensure reproducibility of results. These conditions were selected as representative of the conditions that could be encountered in a potential industrial posttreatment process of gasoline desulfurization.

Because of the low sphericity of the pellets, the catalyst loaded in the basket was a mixture of 0.2 g of H−ZSM-5 catalyst and 1.2 g of 42-μm glass particles (spheriglass, Potter Industries) to achieve better fluidization in the reactor.

3. Results and Discussion

3.1. Catalyst Characterization. XRD analyses were performed on the H−ZSM-5 zeolite, the catalyst pellets, and kaolin. Figure 3 shows the XRD pattern for the H−ZSM-5 zeolite used in the present study, which is in agreement with previous a report.[22] The patterns and peak intensities are very similar, confirming that the crystals were indeed those of H−ZSM-5 zeolite, with the shift in the positions of the peaks being the result of the different sources of X-rays used in the studies.

Figures 4 and 5 display the XRD patterns for kaolin and H−ZSM-5 pellets, respectively. Although kaolin has a crystalline structure, the dominant pattern in the catalyst pellet that

Table 1. BET Specific Surface Areas (SSAs) for H−ZSM-5 Zeolite, H−ZSM-5 Pellet, and Matrix

sample	SSA (m^2/g)
H−ZSM-5 zeolite	265.6
H−ZSM-5 pellet	132.3
matrix	68.6

Table 2. Results of SEM-EDX Analyses (in atom %). for Na−ZSM-5 Zeolite, H−ZSM-5 Zeolite, and H−ZSM-5 Pellet

element	Na−ZSM-5 zeolite	H−ZSM-5 zeolite	H−ZSM-5 pellet
Si	41.03	42.03	33.96
Al	1.86	1.98	9.74
O	56.13	55.99	55.91
Na[a]	0.90	<0.5	<0.5
Si/Al	22.06	21.23	3.49

[a] The lowest level detected by the instrument is 0.5%.

remains is that of H−ZSM-5 zeolite, given the fact that kaolin collapses after calcination.

For both the H−ZSM-5 zeolite and the H−ZSM-5 pellet, the BET specific surface areas (Table 1) are in good agreement with the previously measured values obtained by Fournier.[23] The specific surface area of the pellet is lower than that of the zeolite (132.3 and 265.6 $m^2\ g^{-1}$, respectively) because kaolin and sodium silicate do not contribute significantly to the final surface area of the catalyst. The specific surface area of the catalyst pellets, made of silica matrix only, is 68.6 $m^2\ g^{-1}$.

Table 2 reports the elemental compositions found for Na^+−ZSM-5 zeolite, H−ZSM-5 zeolite, and H−ZSM-5 pellet using SEM-EDX.

The Si/Al ratio observed for the zeolite before pelletization was 21. For the H−ZSM-5 pellet, however, the presence of kaolin and sodium silicate changed the overall Si/Al ratio to 3.5. In addition, it was observed that the sodium contents of the H−ZSM-5 zeolite and the H−ZSM-5 pellet were below the detectable limits (<0.5%).

SEM images (5000× magnification) showed that the catalyst particles obtained using the gel-and-grind technique had a low sphericity. For a catalyst to display good fluidization, catalyst particles not only have to have a size within the 38−106-μm range, but also have to have adequate sphericity. Thus, to counter this problem and to be able to fluidize the catalyst particles well, mixtures of the catalyst with 42-μm glass particles were employed.

Zeolite catalysts are frequently characterized using the temperature-programmed desorption of ammonia (TPD-NH_3).[24] TPD-NH_3 allows the determination of the total acidity and nature of the acid sites of the samples to be studied. Figure 6 displays the resulting TPD chromatograms for the three samples, and Table 3 summarizes the total acidities. Moreover, it can be observed that both weak acid sites (peaks located at 200 °C) and strong acid sites (peaks located at 420 °C) were found in both the zeolites and the pellets. It was found that the matrix pellet has a low acidity, with the zeolite being the component that accounts for the main activity of the catalyst.

3.2. Chemical Equilibrium Calculations. As postulated by Chang and Silvestri,[7] methyl mercaptan reacts over H−ZSM-5 catalyst following a reaction path similar to that of methanol. Hence, it can be expected that sulfur-containing hydrocarbon molecules will react over ZSM-5 with a reaction path comparable to that of their analogous oxygenate species. These reactions can be considered in the context of thermodynamics equilibrium to develop chemical equilibrium calculations.

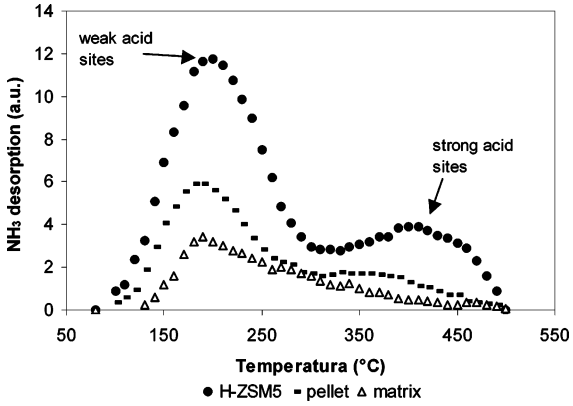

Figure 6. TPD analyses of H−ZSM-5 zeolite, H−ZSM-5 pellet, and matrix.

Table 3. Total Acidities for H−ZSM-5 Zeolite, H−ZSM-5 Pellet, and Matrix

sample	acidity (mmol of NH_3/g)
H−ZSM-5 zeolite	0.70
H−ZSM-5 pellet	0.35
matrix	0.15

(a) Intramolecular Dehydrosulfidation. Ethyl mercaptan reacts via intramolecular dehydrosulfidation to give ethylene and H_2S

$$CH_3{-}CH_2SH \leftrightarrow CH_2{=}CH_2 + H_2S \quad (1)$$

(b) Intermolecular Dehydrosulfidation between Reacting Two Mercaptan Molecules. This reaction leads to the removal of a H_2S molecule from two mercaptan molecules, yielding diethyl sulfide (DiE-S) and H_2S

$$CH_3{-}CH_2SH + CH_2SH{-}CH_3 \leftrightarrow CH_3{-}CH_2{-}S{-}CH_2{-}CH_5 + H_2S \quad (2)$$

Moreover, following this first step, a second reaction step involves further dehydrosulfidation of diethyl sulfide (DiE-S), yielding an olefin (butene) and H_2S

$$CH_3{-}CH_2{-}S{-}CH_2{-}CH_3 \leftrightarrow CH_3{-}CH_2{=}CH_2{-}CH_3 + H_2S \quad (3)$$

Hysys, a commercial process simulator software developed by Hyprotech, was used to aid in equilibrium constant and equilibrium composition calculations of the proposed set of three simultaneous reactions for the dehydrosulfidation of ethyl mercaptan (EM). Calculations were performed using the same operating conditions (temperature, pressure, reactant concentration) as used during experimental studies. Additional details on the chemical equilibrium calculations can be found in the work by Hernandez Enriquez.[25]

The chemical equilibrium constants for the three reactions are reported in Table 4. Reactions 1 and 3 are endothermic reactions, whereas reaction 2 is exothermic. All equilibrium constants are greater than 1; thus, all three reactions are thermodynamically favored under the selected operating conditions.

Regarding the three reactions involved, reactions 1 and 2 are of the competitive type, whereas reactions 2 and 3 are in series. Thus, the overall reaction scheme of dehydrosulfidation is a combined parallel−series reaction network with three reactions contributing to the product distribution.

Table 4. Equilibrium Constants in the 350−500 °C Temperature Range for the EM Dehydrosulfidation Reactions (Eqs 1−3)

T (°C)	K_1 (eq 1)	K_2 (eq 2)	K_3 (eq 3)
350	4.4	3.0	412.7
375	8.1	2.9	695.0
400	14.7	2.8	1136.2
425	25.4	2.8	1808.8
450	42.8	2.7	2811.9
475	70.0	2.7	4278.6
500	111.7	2.6	6385.6

Table 5. Conversion of *n*-Octane at Different Temperatures for Thermal Runs[a]

temperature (°C)	conversion of *n*-C_8 (%)	$(M - M_0)/M_0$ (%)
350	0	5.47
400	0	3.12
450	0.34	7.80

[a] Reaction time: 60 s. Feed: 0.08 g of *n*-octane. Conversions and $(M - M_0)/M_0$ closures are averages of three repeat runs.

Furthermore, observing the calculated equilibrium constants, it can be noted that, for the temperature range studied, the equilibrium constants for reaction 1 are consistently higher than the equilibrium constants for reaction 2, and the equilibrium constants for reaction 3 are much higher than thosefor both reactions 1 and 2. This shows that there is no thermodynamic restriction for the diethyl sulfide species formed to be consumed completely.

In this respect, calculated equilibrium compositions and conversions indicate that, in all cases, the equilibrium conversion is at least 99%, confirming that these reactions are not equilibrium limited.

3.3. Reactivity. 3.3.1. Thermal Runs Using Pure *n*-Octane. Thermal runs were performed using a reaction time of 60 s and three temperatures: 350, 400, and 450 °C. A sample of 0.08 g of pure *n*-octane was injected into the reactor for each run. These conditions were studied to evaluate the influence of thermal reactions under the worst possible scenario (i.e., highest possible *n*-C_8 conversions).

Results of the thermal experiments are reported in Table 5. For each set of conditions, both the conversion and the $(M - M_0)/M_0$ closure are average values for three repeat runs.

Experiments performed with pure *n*-C_8 at both 350 and 400 °C for 60 s, the largest reaction time studied, showed no chemical species from *n*-C_8. This result confirms that, at 400 °C and below, there is no significant *n*-C_8 thermal conversion. Furthermore, at 450 °C and 60 s, a very small amount of *n*-C_8 is converted to ethane and propene, with this fraction being limited to 0.34%. In addition, ethene is present in a larger fraction than propene (0.21 and 0.13 wt %, respectively), with this product distribution being characteristic of thermal cracking where dominant β-scission cracking promotes ethene as the more abundant product.[26]

Table 5 also reports $(M - M_0)/M_0$ closures, with these balances (below 7.8%) being well in the range of typical closures achieved in the CREC riser simulator.[23,27]

Thus, on the basis of the data reported, thermal cracking is neglected, even for the worst possible scenarios (450 °C and 60 s). Under these conditions, the *n*-C_8 conversion observed during the catalytic runs (catalyst loaded) truly represents a result of the ZSM-5 catalyst effects only.

3.3.2. Thermal Runs Using 10 wt % Ethyl Mercaptan in *n*-Octane. The results of thermal cracking with EM and *n*-C_8 mixtures (10 wt % EM/*n*-C_8) are summarized in Table 6. The selected operating conditions were the same as in the previous section, in order to have the highest possible conversions. For these runs, it was found that there is no evidence of conversions of either *n*-C_8 or EM at 350 and 400 °C after 60 s. When the temperature was increased to 450 °C, the *n*-C_8 conversion remained below 1%, which is consistent with the very low conversion observed for *n*-C_8 alone. For EM, however, the conversion was 7.2%. This EM conversion was judged to be modest, considering that these experiments were performed under the reaction conditions (450 °C, 60 s, 10 wt % EM concentration) most favorable to promote undesirable thermal reactions.

Table 6. Conversions of *n*-C_8 and EM at Different Temperatures for Thermal Runs[a]

temp (°C)	conversion of *n*-C_8 (%)	std dev for *n*-C_8 conv	conversion of EM (%)	std dev for EM Conv.	$(M - M_0)/M_0$ (%)
350	0	0	0	0	9.12
400	0	0	0	0	10.51
450	0.60	0.11	7.23	0.90	8.20

[a] Reaction time: 60 s. Feed: 0.08 g of 10 wt % EM/*n*-C_8. Conversion and $(M - M_0)/M_0$ closures are averages of three repeat runs.

Table 7. Product Composition of the Detectable Chemical Species for the Thermal Run in Mass Fraction[a]

species	mass fraction (w_i)
ethene	0.0061
propene	0.0025
trans-/*cis*-butene	0.0017
ethyl mercaptan	0.0928
n-octane	0.8947
hydrogen sulfide	0.0040

[a] Reaction conditions: $T = 450$ °C, $t = 60$ s. Feed: 0.08 g of 10 wt % EM/*n*-C_8.

All of these results also allow one to postulate that any chemical species change observed during the catalytic runs is essentially the result of the ZSM-5 catalytic activity and that there is minimum contribution of thermal cracking.

Despite this very low thermal reaction contribution, it was interesting to review the product species formed, which are reported in Table 7. For a 60-s run at 450 °C with a 10 wt % EM/*n*-C_8 mixture, ethene, propene, and *trans*-/*cis*-butene were the detected products, with ethene being the most abundant species, followed by propene and *trans*-/*cis*-butene.

It was also observed that ethene was present at higher levels in this case than in the thermal conversion of *n*-C_8: 0.61 wt % ethene versus 0.21 wt % propene, or 3 times higher. This suggests that a significant fraction of ethene formed originated via EM conversion, a possible result of intramolecular H_2S removal. Propene, on the other hand, increased form 0.13 to 0.25 wt %, or by a factor of 2, and this points toward a mild sharing of the EM conversion via a reaction likely involving intramolecular H_2S removal and an alkylation step. Finally, these experiments also show the formation of *trans*-/*cis*-butene species, not observed for the *n*-C_8 thermal conversion, and this strongly suggests an EM conversion via intermolecular removal of H_2S. Thus, the observed reaction products strongly support intramolecular and intermolecular reactions both contributing to the EM conversion under thermal conditions.

Another interesting observation from these experiments is the absence of diethyl sulfide species. These species are expected to be formed via intermolecular dehydrosulfidation. However, it appears that these species are very reactive, being formed and quickly consumed so that they remain at nondetectable levels.

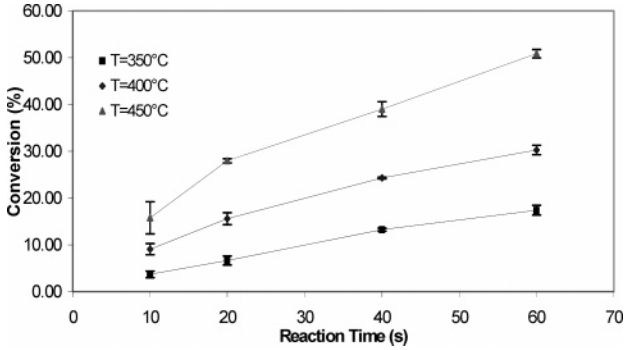

Figure 7. Conversions of ethyl mercaptan versus time. Reaction conditions: T = 350 °C, 400 °C and 450 °C, C/O = 2.5. Feed composition: 10 wt % EM/*n*-C_8. Error bars correspond to standard deviation.

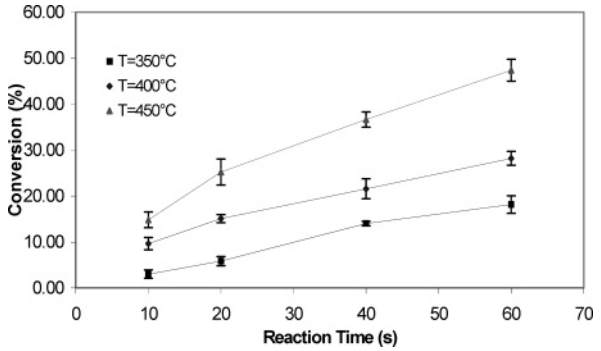

Figure 8. Conversions of ethyl mercaptan versus time. Reaction conditions: T = 350, 400, and 450 °C, C/O = 2.5. Feed composition: 5 wt % EM/95 wt % *n*-C8. Error bars correspond to standard deviations.

Finally, although H_2S could not be detected with the FID, it was positively identified using the GC-MSD, with specific H_2S amounts being quantified via element balances.

3.3.2.1. Catalytic Runs: Conversions of Ethyl Mercaptan. Figure 7 reports EM conversions for the concentration of 10 wt % of EM in *n*-C_8. It can be observed that the EM conversion increases progressively with reaction time in the 10−60-s range. As expected, there is an increase of the dehydrosulfidation reaction given that the EM conversion increased with temperature.

Furthermore, to explore the reaction order of the EM reaction, the content of EM in *n*-C_8 was decreased to 5 wt % keeping the C/O ratio at 2.5. The results of these experiments are reported in Figure 8. From this figure, it can be observed that the EM conversion increases with temperature, leading to maximum conversions close to those obtained with 10 wt % EM in *n*-C_8.

Thus, the lack of dependence of the EM conversions, at various temperatures and reaction times, on the EM concentration (comparison between Figures 7 and 8) suggests a first-order reaction for the EM conversion.

3.3.2.2. Catalytic Runs: Conversions of *n*-*Octane.* The conversions of *n*-octane are reported in Figures 9−11. These figures contain results of experiments performed using 100, 95, and 90 wt % *n*-C_8 (with the balance EM), respectively. It can be noticed that runs show an expected and progressive increase of the conversion with reaction time and temperature. The *n*-C_8 conversions levels, however, remain at much lower levels than for the EM conversion. For instance, at 450 °C, 60 s, and C/O = 2.5, the observed *n*-C_8 conversion is 22.87% ± 0.5% versus 50.85% ± 0.91% for EM under the same conditions.

Thus, this suggests that there is a strong competition for the acid sites of the ZSM-5 catalyst promoting both dehydrosulfidation and catalytic cracking. It appears that, given the significant differences in gas-phase concentrations between *n*-C_8 and EM (between 10 and 20 times), there should be either a greater adsorption affinity of EM versus *n*-C_8 or alternatively a much higher intrinsic rate of EM dehydrosulfidation compared to the *n*-C_8 cracking rate.

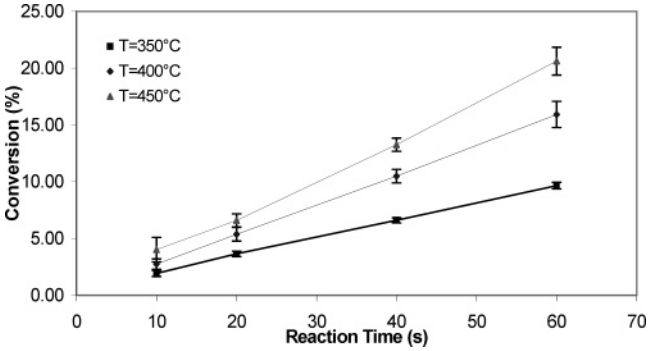

Figure 9. Conversions of *n*-octane versus time. Reaction conditions: T = 350, 400, and 450 °C, C/O = 2.5. Feed composition: 100 wt % *n*-octane. Error bars correspond to standard deviations.

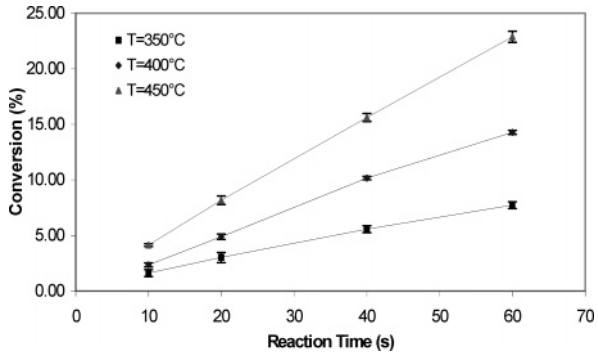

Figure 10. Conversions of *n*-C_8 versus time. Reaction conditions: T = 350, 400, and 450 °C, C/O = 2.5. Feed composition: 10 wt % EM/90 wt % *n*-C_8. Error bars correspond to standard deviations.

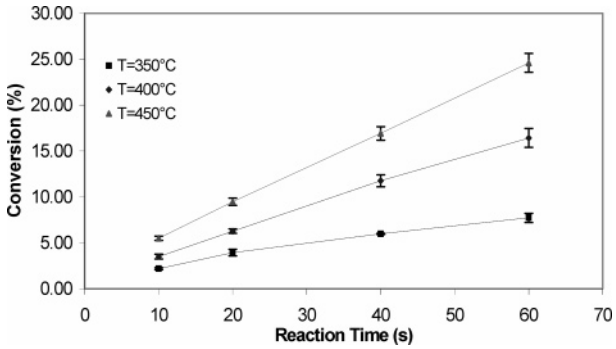

Figure 11. Conversions of *n*-C_8 versus time. Reaction conditions: T = 350, 400, and 450 °C, C/O = 2.5. Feed composition: 5 wt % EM/95 wt % *n*-C_8. Error bars correspond to standard deviations.

3.3.2.3. Catalytic Runs: Product Distribution. As already described, catalytic runs with pure *n*-C_8 always gave propene yields higher than ethene yields, in a ratio of about 7−8:1,[25] with this being a typical characteristic of catalytic cracking.[26] *trans*-/*cis*-Butene during these runs is formed only at 400 and 450 °C and 40 and 60 s, and the amounts produced are very low. On the other hand, the product composition for the catalytic runs using a mixture of EM and *n*-C_8 (Table 8) is richer in *trans*-/*cis*-butene compared to that obtained in runs with pure *n*-C_8. This indicates that EM conversion promotes the formation of *trans*-/*cis*-butene via intermolecular dehydrosulfidation. In addition, it is observed that the hydrogen sulfide produced increases with residence time and temperature, in agreement with the rise of the EM conversion with these two operating

Table 8. Product Distribution of Detectable Chemical Species for Reactions Using 10 wt % EM/*n*-C_8[a]

	time (min)			
	10	20	40	60
	Temperature = 350 °C			
ethane	0.07	0.21	0.46	0.80
propene	0.41	0.71	1.18	1.47
trans-/*cis*-butene	0.00	0.04	0.10	0.19
H_2S	0.34	0.58	1.10	1.42
	Temperature = 400 °C			
ethane	0.20	0.37	0.66	0.80
propene	0.78	1.46	2.80	3.83
trans-/*cis*-butene	0.04	0.08	0.16	0.22
H_2S	0.63	1.12	1.99	2.58
	Temperature = 450 °C			
ethene	0.64	1.06	1.55	1.99
propene	1.35	2.71	4.88	7.14
trans-/*cis*-butene	0.14	0.25	0.40	0.51
H_2S	1.06	1.92	2.86	3.78

[a] Compositions expressed in wt %.

Table 9. *trans*-/*cis*-Butene-to-Ethene ($tcC_4^=/C_2^=$) Ratios for Catalytic Experiments

time	*n*-C_8	EM (5 wt %)	EM (10 wt %)
		T = 350 °C	
10	0	0	0
20	0	0.1976	0.1839
40	0	0.3087	0.2187
60	0	0.322	0.2373
		T = 400 °C	
10	0	0.3322	0.2031
20	0	0.395	0.2074
40	0.117	0.3934	0.244
60	0.2357	0.4197	0.274
		T = 450 °C	
10	0	0.324	0.216
20	0.1059	0.372	0.2354
40	0.1967	0.394	0.2544
60	0.2335	0.4128	0.2559

parameters. Furthermore, the amounts of ethene are also higher for the catalytic runs using mixtures of EM and *n*-C_8 than for runs using pure *n*-C_8. This also provides a good indication that the formation of ethene occurs via intramolecular dehydrosulfidation reaction.

The ratios of *trans*-/*cis*-butene to ethene ($tcC_4^=/C_2^=$), which provide valuable insights on the relative importance of intermolecular and intramolecular catalytic dehydrosulfidation, are reported in Table 9.

It can be noticed that *n*-C_8 conversion leads to $tcC_4^=/C_2^=$ ratios smaller than those observed for EM-*n*-C_8 mixtures. For instance, at 350 °C, this ratio is 0, with no $tC_4^=$ being detected, and with this ratio remaining at low levels at 400 and 450 °C. Thus, on this basis, it can be argued that, at 350 °C, olefin dimerization is negligible, becoming somewhat more prevalent at 400 and 450 °C.

On the other hand, the $tcC_4^=/C_2^=$ ratios increase considerably when the EM/*n*-C_8 mixtures are contacted with the ZSM-5 catalyst. This suggests an increased influence of the competitive conversion of EM via the intermolecular path, with more $tcC_4^=$ species being formed. Thus, there is evidence that, for EM, increasing the temperature leads to a more significant intermolecular EM conversion, with these findings being consistent with the less-reliable reaction order of 1 observed under these conditions.

3.3.2.4. Kinetic Model for the Disappearance of Ethyl Mercaptan. As described in the previous sections, it appears that the EM is being consumed via two competitive reactions: intramolecular and intermolecular dehydrosulfidation. Thus, the total rate of consumption of EM can be viewed as the sum of these two reaction rates. Regarding the intramolecular dehydrosulfidation reaction, it can be assumed to be of first order, a chemical reaction involving a single species. On the other hand, the intermolecular dehydrosulfidation reaction could be considered second-order given that it is the result of the interaction of two sulfur-containing molecules. This view of dehydrosulfidation can be represented as

$$-r_{EM} = k_1 C_{EM} + k_2 C_{EM}^{\ 2} \tag{4}$$

where r_{EM} represents the rate of EM consumption in moles per gram of catalyst per second, C_{EM} is the EM concentration in moles per cubic centimeter, and k_1 and k_2 are the kinetic constants for intramolecular and intermolecular dehydrosulfidation, respectively.

Also, the intermolecular dehydrosulfidation reaction could be considered first-order, with intermolecular dehydrosulfidation being nonelementary. Under these conditions, the overall reaction rate becomes

$$-r_{EM} = k_1 C_{EM} + k_2 C_{EM} = k C_{EM} \tag{5}$$

Equations 4 and 5 contain only catalytic dehydrosulfidation effects, with eventual coke formation and thermal reactions being neglected on the basis of experimental conditions and results obtained in the present study (refer to section 3.4.2).

Equations 4 and 5 can be solved in the context of the CREC riser simulator species balances in conjunction with a quasi-steady-state assumption, as proposed by Atias and de Lasa[28]

$$\frac{dC_{EM}}{dt} = r_{EM}\frac{W_c}{V_r} \tag{6}$$

where W_c is the catalyst weight in grams and V_r is the reactor volume in cubic centimeters.

Substituting eq 5 into eq 6 gives

$$\frac{dC_{EM}}{dt} = -kC_{EM}\frac{W_c}{V_r} \tag{7}$$

Equation 7 can be integrated, and the fractional EM conversion, X_{EM}, can be expressed in terms of both kinetic and operating parameters

$$-\ln(1 - X_{EM}) = \frac{kW_c}{V_r}t \tag{8}$$

Hence, linear regression of eq 10 in a semilogarithmic plot gives the quantity kW_c/V_r. Considering that W_c and V_r are known, the k parameter can be calculated. Table 10 reports the values of k obtained at different temperatures with their 95% confidence limits.

Table 10. Values of the Kinetic Constant at 350, 400, and 450 °C

temperature (°C)	k (cm^3/g_{cat}·s)	95% conf limit	R^2
350	1.11	0.0424	0.9624
400	2.05	0.1169	0.8574
450	3.88	0.1956	0.9184

To obtain both the activation energy and the preexponential factor, the Arrhenius equation can be modified via reparametrization to reduce cross-correlation between parameters. With this end, a central average temperature (T_{av}) is defined as follows

$$k = k_0' \exp\left[-\frac{E}{R}\left(\frac{1}{T} - \frac{1}{T_{av}}\right)\right] \tag{9}$$

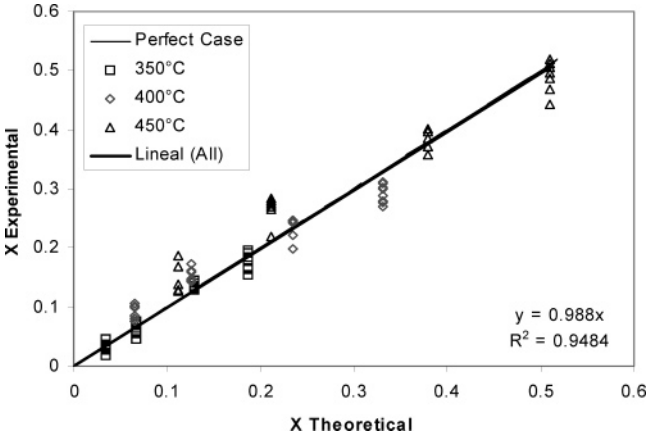

Figure 12. *X* experimental versus *X* theoretical.

where E is the activation energy; k_0' is the preexponential factor, R is the ideal gas constant, and T and T_{av} are the reaction and average temperatures, respectively.

Using eq 9, both the activation energy and the preexponential factor can be calculated via linear regression in a $\ln(k)$ versus $(1/T - 1/T_{av})$ plot. The following values are thus obtained: $E = 46.79 \pm 32.76$ kJ/mol and $k_0' = 9112.48 \pm 359.72$ cm^3/g_{cat}·s.

However, to obtain better estimates of these parameters, a regression can be performed using the following expression

$$X_{EM} = 1 - \exp\left(-\frac{W_c}{V_r} t\left\{k_0' \exp\left[-\frac{E}{R}\left(\frac{1}{T} - \frac{1}{T_{av}}\right)\right]\right\}\right) \quad (10)$$

Equation 10 is a nonlinear relation in terms of k_0' and E. This equation was fitted using a nonlinear regression algorithm,[29] and the kinetic parameters found via linear regression of eq 9 were used as initial guesses. The following are the resulting k_0' and E values, reported with their 95% confidence intervals: $E = 46.66 \pm 34.84$ kJ/mol and $k_0' = 9195.83 \pm 218.75$ cm^3/g_{cat}·s.

Using these constants, the calculated EM conversions (eq 10) can be compared with the experimental data. Figure 12 reports a reasonable random distribution of residuals with a 5.16% linear regression line difference with respect to the 45° perfect-agreement case.

These results indicate that the assumption of a first-order law provides, overall, a good approximation for the EM conversion. There is some deviation of the first-order law at the higher temperatures, however, and this is attributed to the contribution of two factors: (a) an increased influence of the intermolecular conversion of EM, a potentially second-order reaction, and (b) a potential shift in the reaction order for the intermolecular conversion, from first to second, as temperature increases.

Nevertheless, the dominant first-order reaction for the EM conversion is an encouraging finding. It allows speculation that catalytic dehydrosulfidation will be as effective at lower mercaptan concentrations. It can be noticed that this observation is consistent with eq 10, where mercaptan conversion is independent of the initial mercaptan concentration.

4. Conclusions

A H−ZSM-5 catalyst was synthesized and characterized (20 wt % ZSM-5, 40 wt % kaolin, and 40 wt % silica). This catalyst was studied in the context of the dehydrodesulfidation reaction, using ethyl mercaptan dissolved in *n*-octane to represent the contaminated gasoline. The following are the most relevant conclusions of the present study:

(a) The influence of thermal reactions on both the EM and *n*-C_8 catalytic conversions are negligible. The product species identified during the thermal experiments strongly suggest an EM conversion involving intramolecular and intermolecular dehydrosulfidation, with this finding being consistent with thermodynamic equilibrium calculations.

(b) The catalytic EM dehydrosulfidation takes place without hydrogen addition. Both the *n*-C_8 and EM conversions progressively increase with reaction time and temperature. The *n*-C_8 conversions are consistently lower than the EM conversions, indicating a distinctive and favorable selectivity toward EM conversion. Also, the significant differences in gas-phase concentrations between EM and *n*-C_8 point toward a higher adsorption affinity of EM than *n*-C_8 or alternatively a much faster intrinsic rate of EM dehydrosulfidation than *n*-C_8 cracking.

(c) A first-order reaction rate for the EM consumption is proposed here, considering the dependence of the EM conversion on the EM concentration. Applying this model, an apparent energy of activation of 46.66 kJ/mol is calculated.

(d) Product distribution analysis reveals that increasing the temperature in the 350−400 °C range leads to a more significant intermolecular EM conversion, which is consistent with the less-reliable first-order reaction observed at the higher thermal levels.

Acknowledgment

This work was supported with funding from the Natural Sciences and Research Council of Canada and CONICET-Argentina. We express our appreciation to CONACYT-Mexico for support, during the course of this research, of R.H.E. with a postgraduate scholarship. The authors also thank Surface Science Western (SSW) for SEM-EDX analyses and the Department of Geology for X-ray Diffraction studies, both from the University of Western Ontario.

Notation

C_{EM} = EM concentration (mol/cm^3).
E = activation energy (kJ/mol)
k = kinetic constant (cm^3/g_{cat}·s)
k_0 = preexponential factor
k_0' = preexponential factor after reparametrization
k_1 = kinetic constant for the intramolecular dehydrosulfidation (cm^3/g_{cat}·s).
k_2 = kinetic constant for the intermolecular dehydrosulfidation (cm^3/g_{cat}·s).
K_1 = equilibrium constant for eq 1
K_2 = equilibrium constant for eq 2
K_3 = equilibrium constant for eq 3
M = mass of all chemical species at reaction time t (g)
M_0 = Initial mass of chemical species at reaction time $t = 0$ (g)
r_{EM} = reaction rate of EM (mol/g_{cat}·s).
R = ideal gas constant (8.314 J/mol·K)
t = reaction time (s)
T, T_{av} = temperature and average temperature, respectively (K)
V_r = reactor volume (cm^3)
W_c = catalyst weight (g)
X_{EM} = fractional conversion of EM

Acronyms

$tcC_4^=$ = *trans*- and *cis*-2-butenes
MTG = methanol-to-gasoline

Literature Cited

(1) Sutinko, T. Optimal HDS for Lower-Sulfur Gasoline Depends on Several Factors. *Oil Gas J.* **1999**, *97*, 55.

(2) Kaufman, T. G.; Kaldor, A.; Stuntz, G. F.; Kerby, M. C.; Ansell, L. L. Catalysis science and technology for cleaner transportation fuels. *Catal. Today* **2000**, *62*, 77.

(3) Purnell, S.; Hunt, D. A.; Leach, D. Catalytic Reduction of Sulfur and Olefins in the FCCU: Commercial Performance of Davison Catalysts and Additives for Clean Fuels. Presented at the 2002 NPRA Annual Meeting, San Antonio, TX, Mar 17−19, 2002; NPRA Paper AM-02-37.

(4) Babich, I. V.; Moulijin, J. A. Science and technology of novel processes for deep desulfurization of oil refinery streams: A review. *Fuel* **2003**, *82*, 607.

(5) Choi, K.-H.; Kunisada, N.; Korai, Y.; Mochida, I.; Nakano, K. Facile ultra-deep desulfurization of gas oil through two-stage or -layer catalyst bed. *Catal. Today* **2003**, *86*, 277.

(6) Desai, P. H.; Lee, S. L.; Jonker, R. J.; De Boer, M.; Vrielling, J.; Sarli, M. S. Reduce Sulfur in FCC Gasoline. *Fuel Reformulation* **1994**, *43*, 43.

(7) Chang, C. D.; Silvestri, A. J. The Conversion of Methanol and Other O−Compounds to Hydrocarbons over Zeolite Catalysts. *J. Catal.* **1977**, *47*, 249.

(8) MacDougall, L. V. Methanol to Fuels Routes−The Achievements and Remaining Problems. *Catal. Today* **1991**, *8*, 337.

(9) Sedran U.; Mahay, A.; de Lasa, H. I. Modelling Methanol Conversion to Hydrocarbons: Alternative Kinetic Models. *Chem. Eng. J.* **1990**, *45*, 33.

(10) Yurchak, S. Development of Mobil's Fixed-Bed Methanol-to-Gasoline (MTG) Process. *Stud. Surf. Sci. Catal.* **1988**, *36*, 251.

(11) Grimmer, H. R.; Thiagarajan, N.; Nitschke, E. Conversion of Methanol to Liquid Fuels by the Fluid Bed Mobil Process (A Commercial Concept). *Stud. Surf. Sci. Catal.* **1988**, *36*, 273.

(12) Collins, N. A.; Harandi, M. N. McGraw, R. D. Desulfurization of Hydrocarbon Streams. U.S. Patent 5,401,391, 1995.

(13) Collins, N. A.; Harandi, M. N. Desulfurization of Hydrocarbon Streams. U.S. Patent 5,482,617, 1996.

(14) Yu, S. Y.; Waky, T.; Iglesia, E. Catalytic Desulfurization of Thiophene on H−ZSM5 Using Alkanes as Co-Reactants. *Appl. Catal. A* **2003**, *242*, 111.

(15) Biscardi, J. A.; Iglesia, E. Isotopic Tracer Studies of Propane Reactions on H−ZSM5 Zeolite. *J. Phys. Chem. B* **1998**, *102*, 9284.

(16) Biscardi, J. A.; Iglesia, E. Reaction Pathways and Rate-Determining Steps in Reactions of Alkanes on H−ZSM5 and Zn/H−ZSM5 Catalysts. *J. Catal.* **1999**, *182*, 117.

(17) Gabelica, Z.; Blom, N.; Derouane, E. G. Synthesis and Characterization of ZSM-5 Type Zeolites. *Appl. Catal*. **1983**, *5*, 227.

(18) Gianetto, A. Novel Cracking Catalyst for the Production of Reformulated Gasoline. M.E.Sc. Thesis, University of Western Ontario, London, Ontario, Canada, 1993.

(19) de Lasa, H. I. Riser Simulator. U.S. Patent 5,102,628, 1992.

(20) Kraemer, D. Catalytic Cracking of Hydrocarbons in a Riser Simulator: Design and Testing. M.E.Sc. Thesis, University of Western Ontario, London, Ontario, Canada, 1987.

(21) Pruski, J. Adsorption Phenomena during FCC in a Novel Riser Simulator. M.E.Sc. Thesis, University of Western Ontario, London, Ontario, Canada, 1996.

(22) von Ballmoos, R.; Higgins, J. B. Collection of Simulated XRD Powder Patterns for Zeolites. *Zeolites* **1990**, *10*, 313.

(23) Fournier, P. MTBE Synthesis in a Riser Simulator. M.E.Sc. Thesis, University of Western Ontario, London, Ontario, Canada, 1997.

(24) Hidalgo, C. V.; Itoh, H.; Hattori, T.; Niwa, M.; Murakami, Y. Measurement of Acidity of Various Zeolites by Temperature Programmed Desorption of Ammonia. *J. Catal.* **1984**, *85*, 362.

(25) Hernandez Enriquez, R.; Catalytic De-Hydrodesulfidation of Gasoline, M.E.Sc. Thesis, University of Western Ontario, London, Ontario, Canada, 2003.

(26) Gates, B. C.; Katzer, J. R.; Schuit, G. C. A. *Chemistry of Catalytic Processes*; McGraw-Hill: New York, 1979.

(27) Kraemer, D. Modelling Catalytic Cracking in a Novel Riser Simulator. Ph.D. Thesis, University of Western Ontario, London, Ontario, Canada, 1991.

(28) Atias, J. A.; de Lasa, H. Adsorption and catalytic reaction in FCC catalysts using a novel fluidized CREC riser simulator. *Chem. Eng. Sci.* **2004**, *59*, 5663.

(29) Mathlab Manuals, release 14 with service Package 2, Optimization Toolbox, Least-Square Optimization, Nonlinear Curve-fitting, The MathWorks, Inc.: Natick, MA, 1994−2005.

Received for review June 10, 2005
Revised manuscript received November 7, 2005
Accepted November 15, 2005

IE0506825